Sensors and Materials, Vol. 38, No. 5 (2026) 2567–2582
MYU Tokyo

S & M 4454

Variable-step Speed Control for Train Doors with Low-resolution Encoder Constraints

Chun-Yu Liu,[1] Ming-Tsung Yeh,[2*] Chien-Chi Chiu,[3] and Znu-You Syu[4]

[1]Department of Electrical Engineering, Da-Yeh University,
No. 168, University Rd., Dacun, Changhua 515006, Taiwan
[2]Department of Electrical Engineering, National Chin-Yi University of Technology,
57, Sec. 2, Zhongshan Rd., Taiping Dist., Taichung 411030, Taiwan
[3]Railway System Division, Mechanical and Mechatronics Systems Research Labs,
Industrial Technology Research Institute, 195, Sec. 4, Chung Hsing Rd, Chutung, Hsinchu 310401, Taiwan
[4]National Chung Shan Institute of Science and Technology,
No. 300-5, Lane 277, Xi'an St., Xitun Dist., Taichung, Taiwan

(Received June 2, 2025; accepted November 27, 2025)

Keywords: variable-step control, train door speed control, PWM duty cycle control, speed encoder sensor

In metropolitan rail systems, passengers must board and alight expeditiously, rendering the precise control of door opening and closing times imperative for operational efficiency and safety. According to the European standard EN14752, the operational time of train doors must be adjustable within 3 to 5 s. However, the localization and system renewal plan necessitates upgrading the existing door control system without modifying the door mechanism or motor, which poses challenges to system stability and control accuracy. The low resolution of the motor encoder has been demonstrated to impede the efficacy of traditional current-based control methodologies, resulting in sluggish responses and significant challenges in accurately regulating the door's motion to meet regulatory requirements. The development of an optimal method within the constraints of the existing hardware architecture to enhance the effective utilization of their sensing signals is challenging. In this study, we propose a variable-step speed control strategy, which is a simple yet efficient control method that does not require replacing existing sensing devices. The designed system utilizes the speed encoder to estimate real-time speed and implements pulse-width modulation (PWM) duty cycle adjustment for closed-loop speed control. The system dynamically adjusts the step size of the PWM duty cycle on the basis of the magnitude of the speed error. In the case of larger errors, a larger step size is employed to approach the target speed expeditiously. Concurrently, fine adjustments are implemented to ensure smooth operation and mitigate overshoot for minor errors. This method effectively overcomes the limitations caused by low encoder resolution, enhances the stability and reliability of door movement, and ensures compliance with safety regulations. Experimental results show that the door opens within 3.5 s, complying with safety regulations. This indicates that the proposed method facilitates the opening and closing of metro train doors within 5 s, thereby adhering to the established EN14752 standard. This approach offers a cost-effective and reliable solution for metro train door control.

*Corresponding author: e-mail: mtyeh@ncut.edu.tw
https://doi.org/10.18494/SAM5764

ISSN 0914-4935

1. Introduction

Rail transportation is one of the core modes of public transit and plays a critical role in modern urban mobility. During train operation, passengers must rapidly board and alight through side doors. Statistics indicate that 30 to 40% of train operation failures occur in the door system,[1] making door system safety and operational stability essential. According to the European standard EN14752, train doors must meet specific requirements concerning the duration of opening and closing, as well as the closing force. These requirements are designed to ensure passenger safety and operational efficiency.

This study is focused on double sliding powered doors, which are designed to protect passengers during train movement and significantly reduce delays caused by door malfunctions. However, under the domestic system replacement plan, existing door control systems and hardware components must be reused to reduce costs and maintain system architecture. Since the motors and encoders still rely on technology from 30 years ago and suffer from limited resolution, conventional control methods are incapable of fine adjustments. Additionally, the train door's travel distance is only 1.2 m, posing a technical challenge to achieving stable and accurate motion within this limited range.

Brushless DC (BLDC) motors are widely used in train door systems owing to their simple structure, high power density, and high reliability.[2,3] In the field of door control, He and Wang proposed a controller based on a mathematical model to drive BLDC motors.[4] Wang *et al.* analyzed and optimized current and velocity closed-loop control strategies based on three schemes.[5] Lv *et al.* developed a flexible variable structure (FVS) controller to enhance the dynamic and static performance of BLDC motors in aerospace electric actuator (EA) systems.[6] Fang *et al.* improved motor responsiveness and torque through compensator-based torque control.[7] In other works, such as Ref. 8, parameter-optimized motion curves were introduced to improve traditional acceleration and deceleration strategies, while infrared sensors were added for precise motor control in Ref. 9.

Although these methods demonstrate outstanding control performance in theory and practice, they are generally unsuitable for legacy hardware environments. The motor and encoder are outdated and have insufficient resolution and accuracy, making current-based or torque-compensated control methods challenging to implement. Kovudhikulrungsri and Koseki introduced a dual-sampling-rate observer to accurately estimate motor speed and disturbances at low speeds with low-resolution encoders.[10] Still, this method requires dual observers, resulting in a complex hardware design. Petrella *et al.* explored various advanced speed estimation algorithms to achieve precise control,[11] but these approaches demand significant system resources and fast computation. Akrami *et al.* conducted a review of the use of low-resolution Hall position sensors in permanent magnet synchronous motor control and position estimation, thereby providing valuable insights into control accuracy and signal processing under limited sensor resolution,[12] yet its complexity and high resource requirements make it less suitable. Wu *et al.* presented an asynchronous sampling pulse method (ASPM) for low-speed or variable-speed systems using low-resolution encoders.[13] Still, this method is unsuitable for short-range (1.2 m) door control tasks. A hardware-based velocity estimation method was proposed for

robotic systems under low-resolution encoders by Callico *et al*., which led to complexity in the hardware design.[14] Bellini *et al.* proposed a digital filtering algorithm based on a static Kalman filter. However, it estimates velocity through differentiation; it is prone to noise at low speeds and requires further filtering to be effective.[15]

Because of the above hardware limitations, directly applying existing methods may not yield optimal results. Therefore, in this study, we propose a practical and straightforward variable-step speed control method. By dynamically adjusting the pulse-width modulation (PWM) duty cycle, the system achieves stable speed control without relying on high-resolution encoders, ensuring smooth and accurate train door operation.

2. Simulation of the Train Door System's Modularization and Operation

In this work, the Simulink tool of MATLAB is employed to construct a simulation module of the train door system, which encompasses the torque control and mathematical model of the train door DC motor. The overall train door simulation system is constructed in accordance with the mechanical structure of the train door system. The data outputs of train door operation are generated by simulation under different control modes, and the performances of the simulations are compared.

2.1 Modeling of the train door system

We developed a modular simulation model of the motor and mechanical components in MATLAB to replicate the actual operation of the train door system. The model's design is aimed at guaranteeing that the implemented architecture aligns with the EN14752[16] standard regarding door torque and performance, thereby realizing a control strategy that optimizes the balance between safety and efficiency.

First, a DC motor model is constructed using the Simscape physical modeling module in MATLAB Simulink. The model consists of the following two parts:

- Electrical equivalent circuit: This is composed of resistance (R), inductance (L), back electromotive force (e), and current (i).
- Mechanical model: This includes moment of inertia (J), angle (θ), angular velocity ($\dot{\theta}$), motor output torque (T), and friction ($b\dot{\theta}$).

A mathematical representation of the DC motor is derived by integrating the electrical equivalent circuit and free-body force analysis, as depicted in Fig. 1.[17]

Equations (1) through (11) are derived to mathematically model the dynamic behavior of the DC motor.[17] The initial step in this process is to derive the correlation between motor torque and the current in the armature coil. In accordance with the Lorentz force principle, the flow of current through conductors, such as an armature coil situated within a magnetic field, gives rise to the generation of a force that, in turn, results in the production of torque. This phenomenon can be succinctly expressed by Eq. (1), which illustrates the linear relationship between torque and current.

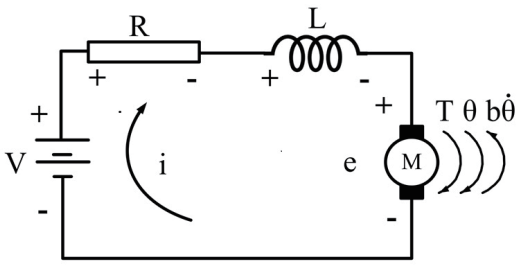

Fig. 1. Equivalent circuit of the DC motor.

$$F = B * I * \ell \tag{1}$$

Here, B represents the magnetic field strength, I is the current, and ℓ is the length of the conductor.

In this model, the magnetic field strength and the effective length of the current-carrying conductor collectively affect the Lorentz force acting on the conductor. This, in turn, affects the generated torque. If multiple armature conductors form a closed loop, the forces produced by each conductor are combined into a total resultant force. The collective expression of this phenomenon is represented by[17,18]

$$T = \sum F * r = C_t * i\,, \tag{2}$$

where F is the force, r is the lever arm, C_t is the torque constant, and i is the current.

Subsequently, we derive the relationship between the back electromotive force (e) and angular velocity. According to Faraday's law of electromagnetic induction, the electromotive force (EMF) can be expressed as shown in Eq. (3). In this equation, N signifies the number of turns in the coil and Φ represents the magnetic flux per turn.

$$e = N\frac{d\Phi}{dt} \tag{3}$$

When the motor rotates, the rotor spins within a magnetic field, and the induced EMF can be described by Eq. (4). If the magnetic flux density (B) remains constant, the rate of change in magnetic flux ($\frac{d\Phi}{dt}$) varies with angular velocity, meaning $\frac{d\Phi}{dt} \propto \dot{\theta}$. Then, the result is substituted into Eq. (3), resulting in Eq. (5).[17,18]

$$\Phi = B * A * \cos\theta \tag{4}$$

$$e = C_e\dot{\theta} \tag{5}$$

Subsequently, e is proportional to the rotor's angular velocity ($\dot{\theta}$) through a proportional constant (C_e). Equation (4) establishes a clear mathematical relationship that describes the back EMF generated by the motor during rotation. Next, according to Newton's law of motion, the torque acting on the rotor can be derived. It is hypothesized that the net torque acting on the rotor is equivalent to the change caused by its angular velocity. The mathematical expression is given by Eq. (6), where J is the moment of inertia of the rotor, θ is the angle, T_{net} is the net torque, T is the applied torque, and $b\dot{\theta}$ represents the friction.[17,18]

$$T_{net} = J\frac{d^2\theta}{dt^2} = T - b\dot{\theta} \tag{6}$$

If $\frac{d^2\theta}{dt^2}$ is integrated, the angular velocity can be obtained as shown in Eq. (7). Substituting Eq. (7) into Eq. (6) results in Eq. (8).[17,18]

$$\int \frac{d^2\theta}{dt^2} = \frac{d\theta}{dt} = \dot{\theta} \tag{7}$$

$$J\frac{d^2\theta}{dt^2} = T - b\dot{\theta} \rightarrow \frac{d^2\theta}{dt^2} = \frac{1}{J}\left(C_t i - b\frac{d\theta}{dt}\right) \tag{8}$$

Next, we utilize Kirchhoff's Voltage Law to analyze the circuit loop in Fig. 2, thereby deriving the relationship among voltages. The resulting expression is shown as[17,18]

$$V = +Ri + L\frac{di}{dt} + e\,. \tag{9}$$

The integration of $\frac{di}{dt}$ is performed as in Eq. (10). Then, substituting Eq. (10) into Eq. (9) results in Eq. (11).[17,18]

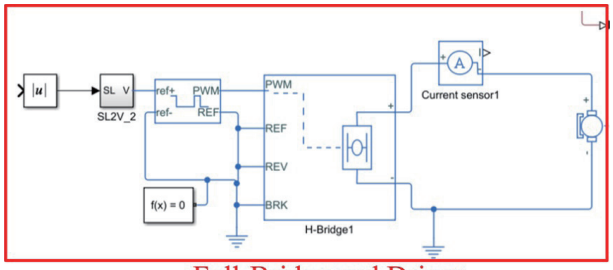

Full-Bridge and Driver

Fig. 2. (Color online) Controller and driver modules of DC motor in Simscape simulation.

$$\int \frac{di}{dt} dt = i \tag{10}$$

$$L\frac{di}{dt} = -Ri + V - e \rightarrow \frac{di}{dt} = \frac{1}{L}\left(-Ri + V - C_e\dot{\theta}\right) \tag{11}$$

The torque of a DC motor is directly related to its current, as demonstrated in Fig. 2. Upon the input of a desired control command, the system employs a limiter to restrict the motor's maximum output, thereby ensuring that its operation remains within the predetermined control range. The variable-step speed controller is responsible for calculating the duty cycle of the PWM signal and outputting it to the H-bridge driver circuit, which in turn controls the operation of the DC motor. To prevent the PWM duty cycle from reaching its maximum value, the controller's output is proportionally scaled and limited to a range of 20–95%. This enhances control stability and system reliability.

A complete door construction system consists of a DC motor with an attached gearbox to amplify the motor's torque, a pinion, and a mechanical linkage to convert the rotary motion into a linear motion of the door. The motor is connected to a lead screw via coupling to ensure a stable and smooth operation of the overall structure. The system also includes left- and right-facing doors mounted on movable guide rods. To achieve a comprehensive simulation of the door's opening and closing movements, we employ Simscape Multibody components to construct the entire door system, as depicted in Fig. 3. To enhance the realism of the simulation, a mechanical friction block is incorporated into the gearbox to react more authentically to various obstacles and frictional forces during the door's operation.

2.2 Simulation of the door moving process

According to the EN14752 standard, train door opening and closing operations must be completed within 3 to 5 s to ensure passenger boarding and alighting efficiency and safety. We

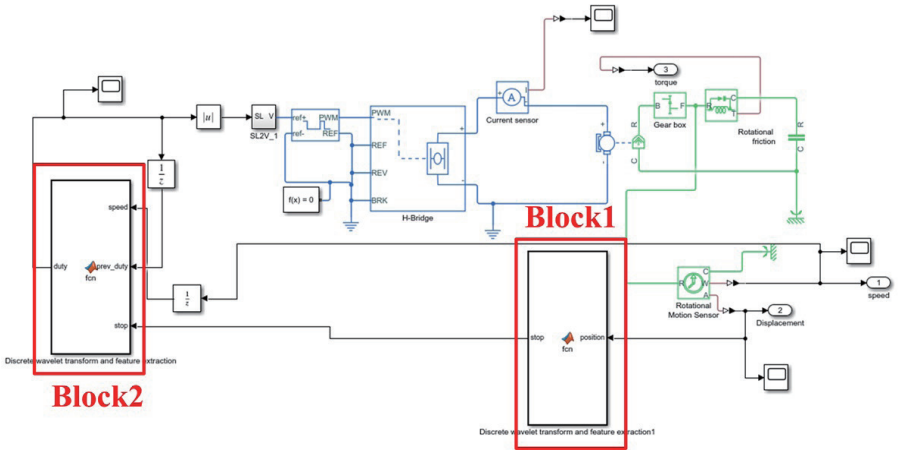

Fig. 3. (Color online) Simscape-based simulation model of a railway train door system.

conduct a dynamic simulation of the doorclosing process and adopt a segmented speed control strategy, dividing the closing motion into five speed intervals. Each interval is precisely controlled to ensure that the door operation time complies with regulatory requirements.

In this study, the EN14752 standard requires the door opening and closing process to be completed within 3 to 5 s. However, to observe the entire process during simulation, the simulation duration was set between 4 and 12 s, incorporating adjustments across different speed intervals to evaluate the adaptability of the control system under various load and boundary conditions, as well as the simulation setup and results. During the speed control process, variable-step speed regulation and PWM duty cycle adjustment are applied to stabilize speed variations, resulting in smoother door operation. The feedback rotational speed is obtained through the designed DC motor model to ensure that the control system can monitor the motor's operating status in real time and adjust the torque output on the basis of the actual performance.

Subsequently, function block 1 is defined in the simulation model and employed to emulate the door reaching the boundary. The system is designed to trigger a stop signal when the distance of door travel reaches 120 mm, thereby simulating the scenario in which the door reaches its boundary and necessitates the cessation of movement. This ensures that the door decelerates and stops appropriately upon full closure, thereby preventing overshoot or mechanical impact.

Function block 2 is configured for speed regulation and PWM duty cycle adjustment. The PWM duty cycle is controlled by a five-stage speed regulation strategy, enabling the precise tracking of speed variations. When the door speed deviates from the target value, the system dynamically compensates for the speed error by appropriately adjusting the PWM duty cycle. This ensures smooth door operation and compliance with the required opening and closing time standards.

We aim to design a speed control mechanism of the door motor with a control interval of 100 ms, given the low resolution of the motor's encoder in the old door system. Therefore, the speed calculation and adjustment are performed every 100 ms to ensure the stability and accuracy of the door opening and closing process. In each control cycle, the system performs the following steps:

(1) Calculate current speed:

The system computes the current speed of the motor.

(2) Determine speed difference:

The speed difference (ΔV) is calculated by comparing the current speed with the target speed to obtain the control error.

(3) Three-stage duty cycle adjustment based on speed error

- Very large error (ΔV > Very large) → Perform an extreme duty cycle adjustment to apply a strong correction and rapidly approach the target speed; suitable for initial startup or severe speed deviations.
- Large error (Very large > ΔV > large) → Apply a large duty cycle adjustment to quickly converge to the target speed and shorten the settling time; used during the acceleration phase.
- Moderate error (Large > ΔV > Medium) → Perform a moderate duty cycle adjustment to gradually stabilize the speed and avoid excessive compensation that may lead to oscillation; applicable when the speed is nearing the steady state but still deviates notably.

- Small error (Medium > ΔV > Small) → Apply a small duty cycle adjustment to reduce overshoot and maintain smooth operation; suitable for fine corrections.
- Very small error ($\Delta V \leq$ Small) → Apply a minimal duty cycle adjustment to maintain the target speed and ensure system stability; used during steady-state operation for minor compensation.

(4) Duty cycle limits:

Upper and lower bounds for the PWM duty cycle are defined to ensure that the signal remains within a safe operating range, preventing motor overload or instability.

(5) Return to main program:

After the adjustment, the system returns to the main program and waits for the next 100 ms control cycle.

The variable-step control defines four adjustment levels—Very large (25%), Large (10%), Medium (5%), and Small (1%)— on the basis of the speed error. A larger duty step (25%, 10%) is used to rapidly overcome static friction and shorten rise time, while smaller steps (5%, 1%) are applied near the target speed to avoid oscillations and ensure smooth steady-state operation. This design balances fast convergence with stable performance under low-resolution encoder constraints.

The proposed method integrates a low-resolution encoder with a time-interval-based control strategy, ensuring the train door's smooth and standard-compliant opening and closing. Improving the system's adaptability and reliability is pivotal in enhancing its performance. The flowchart and logic block diagram for the variable-step speed control method are shown in Fig. 4.

As illustrated in Fig. 5, the waveform curves depict variations in speed, PWM duty cycle, and motor current during the simulated door opening and closing process, which is facilitated by the implementation of the variable-step control strategy. The speed scale in the simulation result diagram is expressed as the number of encoder pulses within 0.1 s, while the duty cycle is represented as a ratio (e.g., 0.6 corresponds to 60%). The current is measured in units of approximately 1 A per scale. This control method dynamically adjusts the PWM duty cycle on the basis of the error between the current speed and the target speed, ensuring a stable convergence of the speed and compliance with the required door operation and closing time. In the initial stage, the speed rises rapidly from zero. In the low-speed region, larger duty cycle increments are applied to provide sufficient driving force to accelerate the motion. As the speed approaches the target value, the variable-step control gradually reduces the duty cycle adjustment range, allowing the speed to stabilize within an acceptable range.

The experiment with a non-stepped control of the train door operation is performed to compare the effect of this mode with that of the variable-step mode. When a smaller gain of the PWM duty cycle is employed, the system exhibits good steady-state performance; however, it experiences a longer rise time, resulting in slower door opening and closing. As illustrated in Fig. 6, the non-stepped control simulation with low gain demonstrated that the system required approximately 6 s to reach the target speed. The system exhibited a more gradual rise, indicating a sluggish response during the initial startup phase. However, the proposed variable-step control method accomplishes the same objective in approximately 0.5 s. This outcome signifies a

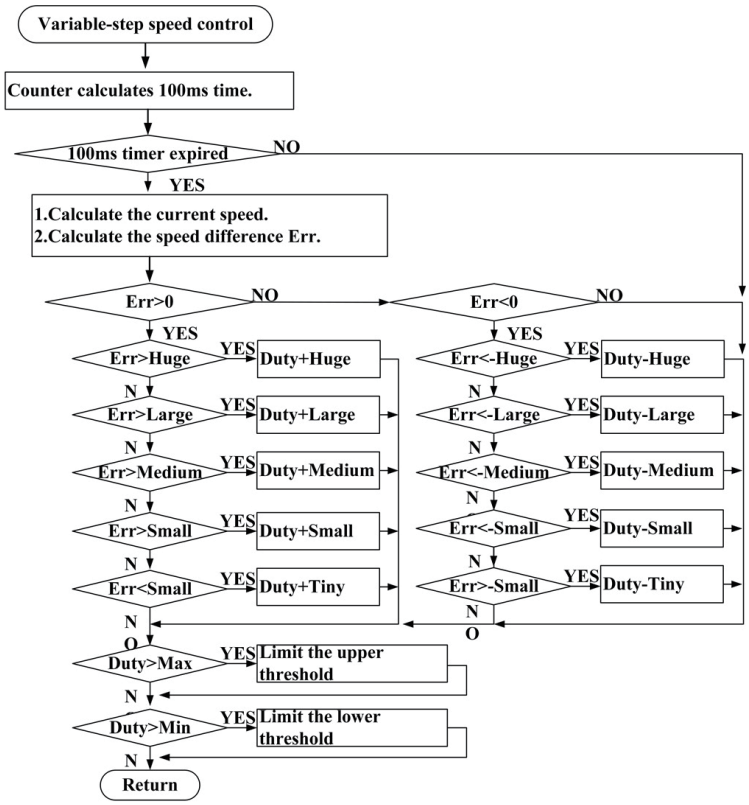

Fig. 4. (Color online) Flowchart and logic block diagram of the variable-step speed control method.

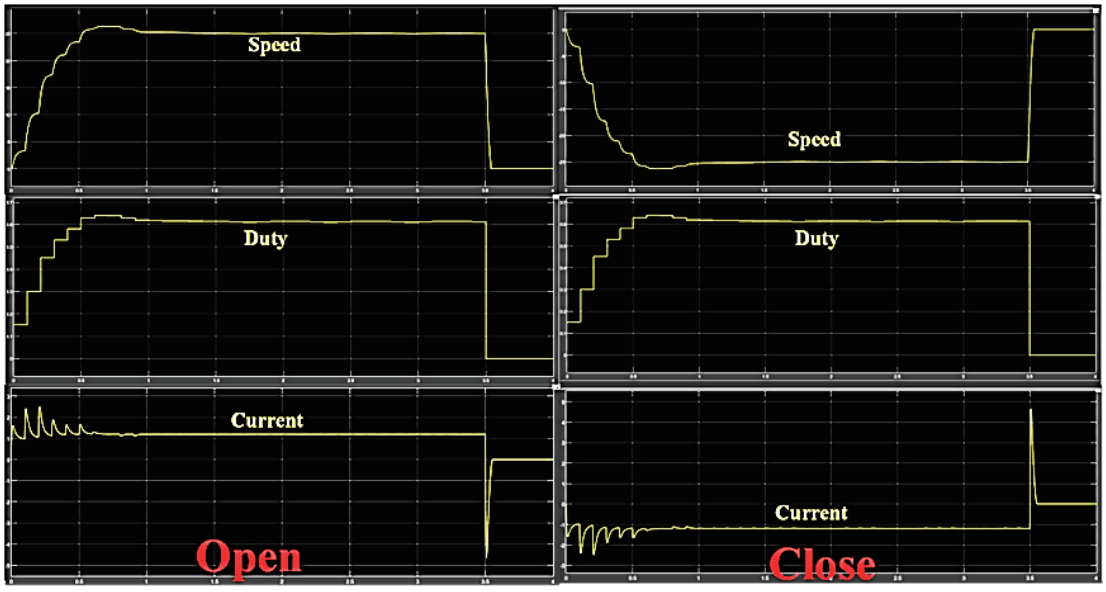

Fig. 5. (Color online) Waveforms of speed, duty cycle, and motor current during simulated door opening and closing under variable-step speed control.

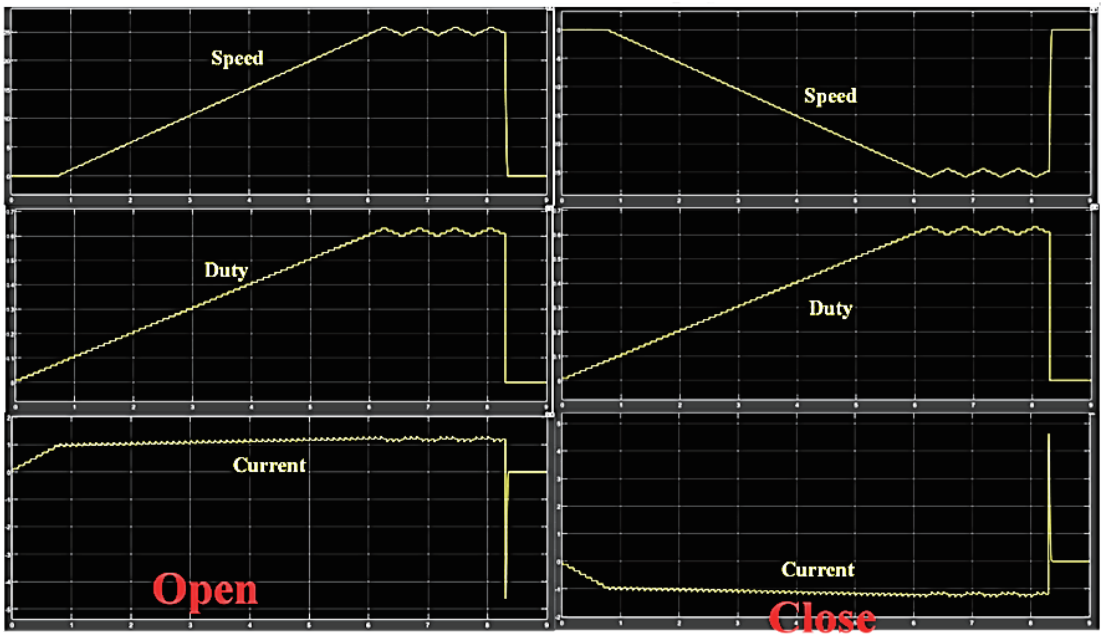

Fig. 6. (Color online) Waveforms of speed, duty cycle, and motor current during simulated door opening and closing under non-stepped control with low gain.

substantial enhancement in dynamic response, approximately 12 times faster than the conventional method. To achieve precise door opening and closing timing, the ideal target speed (defined as 25 pulses per 0.1 s) is realized under a steady-state duty cycle of approximately 60% and a corresponding current of approximately 1.1 A. The simulation results of variable-step control closely approximate the set target.

We also analyze the impact of high-gain PWM duty cycle control on the system performance. While a higher gain may reduce rise time, it can also compromise system stability and lead to oscillations. As illustrated in Fig. 7, the simulation results indicate a rise time of approximately 0.6 s, exhibiting a more rapid ascent than in the previous case. However, upon attaining a steady-state speed, the system displays substantial oscillations, with the actual speed fluctuating around a reference value of 25 pulses per 0.1 s, ranging from +3 to –10. This corresponds to a steady-state error range of approximately +12 to –40%. In contrast, the proposed variable-step control maintained stability near the reference value. This finding highlights the substantial difference in error performance between the two methods. Once the duty cycle has stabilized, it maintains a proximity to 60%, though it displays amplitude variations ranging from approximately +5 to –20%. The corresponding current has been measured to be approximately 1.1 A, with fluctuations between +1 and –0.7 A. These results suggest that, although the rise time is similar, the non-stepped control method is subject to pronounced oscillations and a considerable increase in steady-state error. This indicates that the non-stepped method is less stable than the variable-step approach.

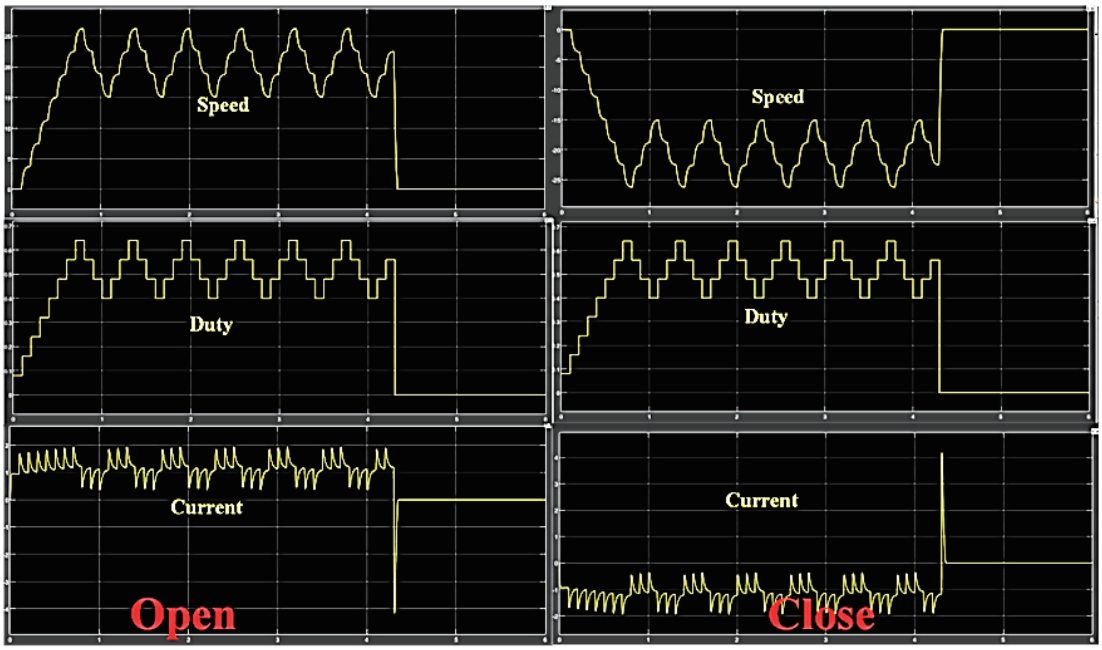

Fig. 7. (Color online) Waveforms of speed, duty cycle, and motor current during simulated door opening and closing under non-stepped control with high gain.

3. Hardware Design

The proposed variable-step speed control method was simulated and validated using a Simscape physical model in the MATLAB environment. The simulated door motor speed, PWM duty cycle, and motor current met the expected requirements. We designed the hardware circuit of the door motor speed control using this algorithm to enable smooth door switching. As shown in Fig. 8, the circuit board is divided into three main sections. Each section is responsible for different functions, ensuring stable system operation and precise motor control.

The upper-left section of the circuit board contains the I/O and analog-to-digital converter (ADC) sensing circuits, which handle digital and analog signal input and monitoring. The I/O interface receives signals from external sensors or devices, and the built-in ADC converts analog data into digital signals for the microcontroller (MCU) to process. This enables real-time system status monitoring and enhances operational reliability. The lower-left section houses the MCU circuit, which includes the microcontroller that processes signals from the sensing circuits, performs logic operations, and controls motor operation via PWM signals. The MCU also manages communication with external devices to ensure coordinated system operation. The right section contains the motor driver circuit, which includes an H-bridge and power MOSFETs that deliver the high-power output required by the motor. Large onboard capacitors and inductors stabilize the current and reduce electromagnetic interference to ensure smooth motor operation. On the basis of the PWM signals output by the MCU, this section adjusts the motor's speed and direction, enabling efficient, stable motor control throughout the system.

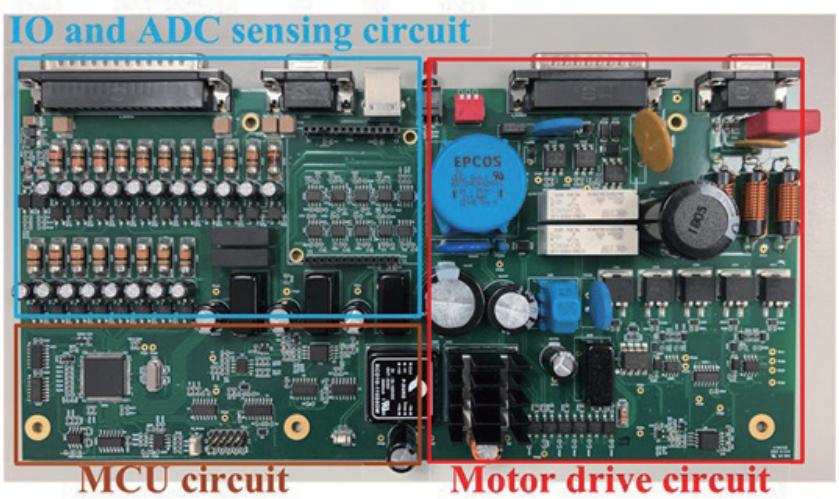

Fig. 8. (Color online) Physical circuit of the train door controller.

Figure 9 shows the schematic diagram of the train door system; the main components, including the door mechanism, door panel, drive linkage, and door control unit (DCU), are illustrated. The door mechanism, located at the top, consists of a drive motor and a sliding rail that ensure smooth door operation. The central door panel is typically made of aluminum alloy or stainless steel for durability and safety. Drive linkages on both sides synchronize the movement of the double doors. The DCU, positioned in the lower right corner, receives control commands and regulates key functions, such as door speed, closing force, and obstacle detection. This ensures that the system operates in compliance with the EN14752 standard.

To test the variable-step speed control method proposed in this paper on an actual door system, a train door testing system was fabricated in the laboratory, as shown in Fig. 10. The system was used to implement and verify the operation of the designed door control board, as well as the door's automatic opening and closing, obstacle detection, and control system stability. The door itself has a double-sliding design with transparent windows that enhance visibility and safety. A touch sensor installed at the center of the door panel simulates passenger interaction to open and close the door.

4. Experimental Results and Discussion

Figure 11 shows the waveforms of the motor current change during the entire door opening process under variable-step speed control in the actual door opening test. The test results indicate an opening cycle of 3.4 s, complying with the EN14752 standard. The current waveform shows an inrush current at startup, followed by a stable operating phase and a rapid drop in current when stopping. This demonstrates effective system control. A comparison of the simulation and experimental waveforms reveals consistent trends, verifying the model's accuracy. However, slight differences in current distribution appear in certain segments owing to the bearing friction and lubrication conditions. An examination of the experimental

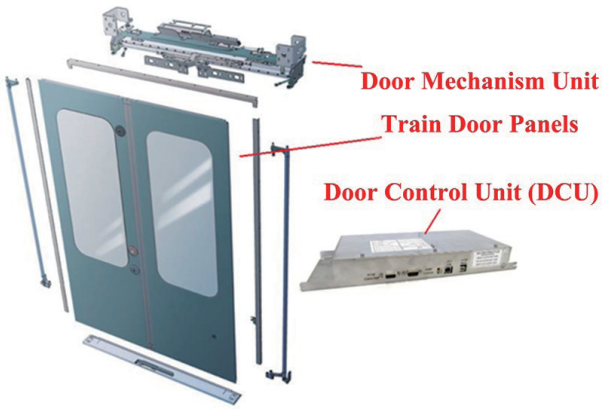

Fig. 9. (Color online) Schematic diagram of the train door system.

Fig. 10. (Color online) Physical view of the train door testing system.

Fig. 11. (Color online) Real motor current waveforms during door opening and closing under variable-step speed control.

waveforms reveals that the door-opening current reaches a steady state at approximately 1 A following the inrush, whereas the door-closing current stabilizes at around 1.5 A after the inrush.

The speed variation during the door opening process was captured in this study via data transmission and logging using the universal asynchronous receiver/transmitter (UART) interface, as demonstrated in Fig. 12. The findings of the test results indicate a close correspondence between the measured speed curve and the simulated waveform, thereby substantiating the precision of the simulation model. The duty cycle variations were additionally observed via data logging to examine PWM modifications during the door opening procedure, as demonstrated in Fig. 13. The measured results indicate a high degree of correlation between the duty cycle adjustments and the simulated waveform trend. It has been determined that, owing to the aging of the door test mechanism's slide rails and gears, a higher duty cycle is required for operation. Consequently, the actual duty cycle in Fig. 13 is higher than the simulated ideal duty cycle. However, the overall speed and duty cycle waveform trends align with the ideal simulation results.

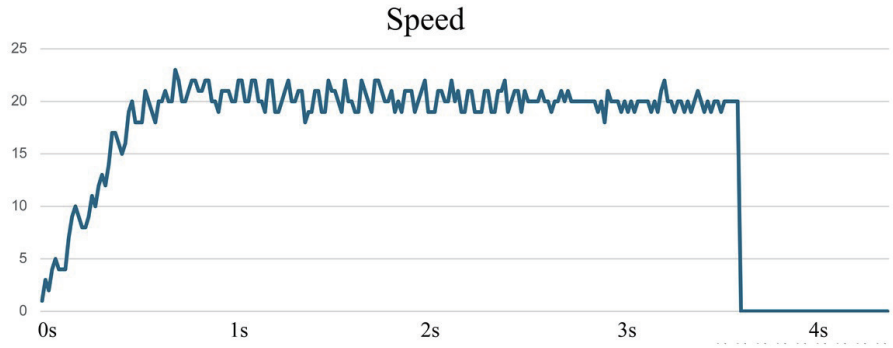

Fig. 12. (Color online) Real speed waveform under variable-step speed control.

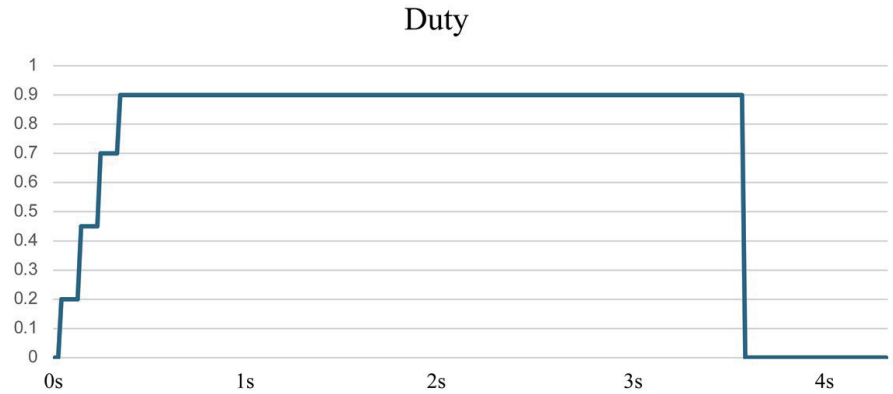

Fig. 13. (Color online) Real duty cycle waveform under variable-step speed control.

The proposed variable-step speed control method was validated through simulation and experiments, demonstrating compliance with the EN14752 standard even under low encoder resolution. The experimental outcomes demonstrated strong alignment with the simulation trends, exhibiting only minor discrepancies in current waveforms that were primarily attributable to friction and lubrication effects. A comparison of the proposed strategy with fixed-step methods revealed that the former achieved faster convergence and reduced oscillations, resulting in smoother door operation. Although this study was limited to an older train door system with a 1.2 m travel distance, the results indicate strong potential for broader applications. Subsequent research endeavors will encompass the examination of disparate door configurations and the incorporation of supplementary sensing technologies, such as force sensing, to further enhance safety and adaptability.

5. Conclusions

In this study, we proposed and implemented a variable-step speed control method, which was validated through Simulink simulations. This method was then compared with fixed single-step strategies (large-step and small-step control) to evaluate its impact on train door opening and closing operations. The results showed that the fixed-step methods are limited in their ability to regulate speed, whereas the proposed variable-step control method dynamically adjusts the PWM duty cycle in accordance with speed error. This enables the system to rapidly converge during acceleration and maintain smooth performance during steady-state operation. A subsequent comparison of simulation and experimental data confirmed the efficacy of the method in controlling railway train doors and complying with EN14752 safety time requirements. The door process was successfully executed within 3.5 s, thereby meeting the regulatory requirements. The final test results demonstrated that the method effectively controls door operation time within the regulatory range. Throughout the process, stable current profiles are maintained, with no occurrence of sudden current surges. This approach was adopted to ensure the safety and reliability of the system.

References

1 F. Turgis, R. Copin, P. Loslever, L. Cauffriez, and N. Caouder: Proc. 2009 ESREL Conf. European Safety and Reliability (CRC, 2009) 21–23. https://scholar.google.com/scholar?oi=bibs&cluster=4128439480455381705&btnI=1&hl=en
2 C. L. Xia and H. W. Fang: Trans. of China Electrotech. Soc. **27** (2012) 25. https://dgjsxb.ces-transaction.com/EN/article/downloadArticleFile.do?attachType=PDF&id=1514
3 J. M. Seo, J. H. Kim, I. S. Jung, and H. K. Jung: IEEE Trans. Ind. Appl. **47** (2011) 730. https://doi.org/10.1109/TIA.2010.2091611
4 Q. He and Y. Wang: Proc. 34th Chinese Control Conf. (IEEE, 2015) 4388–4392. https://doi.org/10.1109/ChiCC.2015.7260319
5 X. Wang, X. Zhang, L. Li, and B. Liu: Proc. 2009 2nd Int. Conf. Intelligent Networks and Intelligent Systems (IEEE, 2009) 589–-592. https://doi.org/10.1109/ICINIS.2009.155
6 Y. Lv, T. Hao, Y. Liu, J. Wang, and Q. Zou: Proc. 2010 IEEE Int. Conf. Mechatronics and Automation (IEEE, 2010) 824–827. https://doi.org/10.1109/ICMA.2010.5589015
7 J. Fang, X. Zhou, and G. Liu: IEEE Trans. Power Electron. **27** (2012) 4952. https://doi.org/TPEL.2012.2193420.
8 C. Li, D. Jiang, J. Yu, and C. Liu: Proc. 2019 22nd Int. Conf. Electrical Machines and Systems (IEEE, 2019) 1–5. https://doi.org/10.1109/ICEMS.2019.8922568

9 T. Koyanagi, S. Inatama, S. Oh, and Y. Hori: Proc. 2010 IEEE Int. Symp. Industrial Electronics (IEEE, 2010) 3571–3576. https://doi.org/10.1109/ISIE.2010.5637960
10 L. Kovudhikulrungsri and T. Koseki: IEEE/ASME Trans. Mechatron. **11** (2006) 661. https://doi.org/10.1109/TMECH.2006.886194
11 R. Petrella, M. Tursini, L. Peretti, and M. Zigliotto: Proc. 2007 Int. Aegean Conf. Electrical Machines and Power Electronics (IEEE, 2007) 780–787. https://doi.org/10.1109/ACEMP.2007.4510607
12 M. Akrami, E. Jamshidpour, and V. Frick: Proc. 2023 IEEE Int. Conf. Environment and Electrical Engineering and 2023 IEEE Industrial and Commercial Power Systems Europe (IEEE, 2023) 1–6. https://doi.org/10.1109/EEEIC/ICPSEurope57605.2023.10194763
13 J. Y. Wu, Z. Chen, A. Deguet, and P. Kazanzides: Proc. 2018 IEEE/RSJ Int. Conf. Intelligent Robots and Systems (IEEE, 2018) 6384–6389. https://doi.org/10.1109/10.1109/IROS.2018.8594139
14 G. M. Callico, A. Nunez, R. P. Llopis, R. Sethuraman, and M. O. de Beeck: Proc. IEEE 2002 28th Ann. Conf. Industrial Electronics Society (IEEE, 2002) 1439–1444. https://doi.org/10.1109/IECON.2002.1185489
15 A. Bellini, S. Bifaretti, and S. Costantini: Automatika **44** (2003) 67. https://core.ac.uk/download/pdf/14380777.pdf
16 BSI Standards Development: Railway applications — Bodyside entrance systems for rolling stock, (British Standards Institution, London UK, 2022) BS EN 14752:2019+A1:2021.
17 Y. Shiao, P. Gadde, and C. Y. Liu: Applied Sciences **15** (2025) 25. https://doi.org/10.3390/app15010025
18 A. Hughes and B. Drury: Electric Motors and Drives, A. Hughes and B. Drury, Eds. (Newnes, Australia, 2019) 5th ed., Chap. 3. https://www.sciencedirect.com/science/article/pii/B9780081026151000039